Journal of Manufacturing Processes 75 (2022) 1144–1152

Contents lists available at ScienceDirect

Journal of Manufacturing Processes

journal homepage: www.elsevier.com/locate/manpro

The effect of cooling on machining and phase transformation responses of Ni-rich NiTiHf high-temperature shape memory alloy

Y. Kaynak [a,b,*], E. Taşcıoğlu [a,c], S. Sharif [b], M.A. Suhaimi [b], O. Benefan [d]

[a] Department of Mechanical Engineering, Marmara University, Goztepe Campus, Kadikoy, 34722 Istanbul, Turkey
[b] School of Mechanical Engineering, Universiti Teknologi Malaysia, 81310 Johor Bahru, Johor, Malaysia
[c] Torun Bakır Alaşımları Metal San.ve Tic. A.Ş., Research and Development Center, İhsan Dede Cad. No:116, 41480, Gebze, Kocaeli, Istanbul, Turkey
[d] Materials and Structures Division, NASA Glenn Research Center, Cleveland, OH 44135, USA

ARTICLE INFO

Keywords:
High-temperature shape memory alloy
Cryogenic machining
Machining performance
Phase transformation
NiTiHf

ABSTRACT

A Ni-rich $Ni_{50.3}Ti_{29.7}Hf_{20}$ (at. %) high-temperature shape memory alloy was machined under different cooling conditions, specifically cryogenic cooling and flood cooling, and results were compared with those from dry machining. The effects of cooling on machinability measures such as tool wear, cutting forces and surface quality were evaluated for various cutting speeds. Microhardness, phase transformation temperatures and latent heat of transformation corresponding to the machined specimens were determined using hardness and differential scanning calorimetry tests. Cryogenic cooling was found to notably improve the machinability of the Ni-rich NiTiHf alloy by reducing tool wear, cutting force and surface roughness. This study provides clear indication that the machining process alters the phase transformation temperature of the Ni-rich NiTiHf alloy. After the machining process, austenite finish temperature of specimens increased by 5–10% depending on the machining conditions. The smallest amount of latent heat required for transformation (ΔH) was obtained for each of the two specimens: 2.33 J/g (exothermic) for the cryogenically machined specimen and 3.38 J/g (exothermic) for the specimen machined under flood cooling.

1. Introduction

Advanced engineering materials such as Ni- and Ti-based alloys are very attractive for aerospace and biomedical applications due to their mechanical and thermal properties. These materials include shape memory alloys (SMAs), namely NiTi SMAs, which have low transformation temperature and therefore do not meet the expectation for high-temperature actuators at elevated temperature [1]. Adding ternary alloying elements such as Zr, Pd, Hf, Pt and Au to NiTi helps to raise the transformation temperature [2] that eventually produces high-temperature SMAs. Such materials have the potential to be used in aerospace, automotive and other engineering industries [3].

Of the few high-temperature SMAs that have been developed, Ni-rich NiTiHf alloys provide notable benefits in terms of dimensional stability [3]. The major concern with this alloy is the need for improvements in manufacturing and fabrication approaches, such as the conventional machining operations that are still being used to develop bulk actuators [4]. Previous studies have reported that SMA properties such as low thermal conductivity, high work-hardening tendency and work-piece stiffness changes (e.g., superelasticity) make machining operation difficult [5–8]. Over time, high tool wear and high cutting forces are commonly observed. Machinability studies of SMAs, particularly NiTi alloys using conventional machining, have been reported by previous researchers [9]. Ni-rich NiTiHf alloys that have higher strength and a high degree of brittleness [10] display significant differences with regard to machinability as compared with NiTi alloys. A recently published comprehensive study on machinability of NiTiHf alloys reported that machining NiTiHf is extremely difficult; the major issue is extremely rapid tool wear, which influences the cutting force and the roughness of machined parts. [11]. An optimization tool is used to determine optimum machining performance [12], but the shape memory properties of SMAs must also be carefully considered to determine the relationship between machining conditions and the resulting properties of the machined part.

Recent studies have investigated the influence of cutting parameters on shape memory and deformation response of NiTi SMAs [13,14]. Because shape memory materials are sensitive to variations in temperature, machining conditions such as cooling also play a critical role in

* Corresponding author at: Department of Mechanical Engineering, Marmara University, Goztepe Campus, Kadikoy, 34722 Istanbul, Turkey.
E-mail address: yusuf.kaynak@marmara.edu.tr (Y. Kaynak).

https://doi.org/10.1016/j.jmapro.2022.01.009
Received 17 October 2021; Received in revised form 9 December 2021; Accepted 2 January 2022
Available online 8 February 2022

determining the shape memory properties of machined parts. Researchers therefore focus on utilizing coolant and lubricant for improving machining performance and for controlling shape memory properties of NiTi alloys [15,16]. Cryogenic cooling and minimum-quantity lubricant (MQL) are two methods researchers prefer to utilize in the machining process of SMAs [17–19], in addition to chilled air system [20]. These studies provide notable evidence that such approaches contribute to improving the machining performance of NiTi SMAs by controlling the phase state of material during the chip removal process, which also positively influences measured surface integrity aspects of the NiTi SMAs.

Studies have also provided evidence that coolant and lubrication, including cryogenic cooling, have a positive effect on machining of other Ni-based difficult-to-machine alloys [21,22]. To the authors' best knowledge, however, this present work is the first study revealing the effect of cryogenic cooling on machinability and resulting shape memory properties of Ni-rich NiTiHf high-temperature SMAs.

2. Method

The work material used was a $Ni_{50.3}Ti_{29.7}Hf_{20}$ high-temperature SMA. The Ni-rich alloy was produced utilizing a vacuum induction skull-melting technique with a heat size of ~27 kg (designated as FS#7). The molten metal was poured into steel molds, and the resulting cast ingots were vacuum homogenized for 72 h at 1050 °C followed by furnace cooling. The material was then canned and extruded at 900 °C through an area reduction ratio of 7:1. The extruded rods were centerless ground to a final diameter of 10 mm and cut into 60-mm-long pieces. The average hardness of the workpiece was 395 ± 5 HV. The transformation temperature of specimens was measured using a Pyris Diamond Differential Scanning Calorimeter at a heating and cooling rate of 5 °C min-1. The tangent-intercept method was used to measure transformation temperature as described by ASTM standards [23]. Differential scanning calorimetry (DSC) samples were cut using a slow-speed diamond saw from the surface/subsurface region of the machined samples. Sample thickness was approximately 300 μm after mechanical polishing. To eliminate the effect of blade cutting, samples were mechanically polished using 800-grit SiC papers before DSC analysis. The NiTiHf alloy was in its martensitic phase at room temperature as determined by DSC, where the martensite start (M_s), martensite finish (M_f), austenite start (A_s) and austenite finish (A_f) temperatures were 88 °C, 64 °C, 112 °C and 130 ± 2 °C, respectively, as shown in Fig. 1(a). A representative microstructure of the workpiece is depicted in Fig. 1(b), illustrating an average grain size of ~36 μm, along with some HfO_2 particles (black dots).

Cutting tests were carried out on a Doosan Puma GT2100 lathe CNC machine with 18 kW power and a maximum spindle speed of 4500 rpm. The feed rate, $f = 0.07$ mm/rev, and depth of cut, $a_p = 0.7$ mm, were kept constant along with three cutting speeds, $V_c = 60$, 90 and 120 m/min. These parameters were used throughout the experimental works considering the optimum parameters presented elsewhere [12]. A DNMG 11 04 04-MF cutting tool insert with 1105-grade TiAlN PVD coating and the PDJNL 2525M 11HP tool holder (Fig. 2d) with a rake angle of $\alpha = -6°$ was used in the machining tests. All the experiments were repeated three times to ensure repeatability and reproducibility of the data.

Three conditions—dry, flood cooling, and LN_2 cryogenic cooling—were used during the tests. Fig. 2 shows images of experimental setups. During the dry cutting, no coolant or lubricant were used. Liquid nitrogen (LN_2) as cryogenic cooling was applied under a pressure of 15 bar. Flood cooling was implemented using XTREME CUT 290 high-performance semisynthetic fluid with a flow rate of 400 l/h and a volumetric concentration of 1:20.

Cutting-force components during the experiments were measured using a three-component piezoelectric KISTLER 2129AA dynamometer. Cutting temperature was recorded using an Optris PI 400 infrared camera. Emissivity of the work material was determined as 0.63. The arithmetical average surface roughness (R_a) of the machined parts was measured with a Mitutoyo SJ210 surface profilometer. Tool wear, surface topography and microstructure were captured using a Keyence VHX-6000 digital optical microscope. A Future-Tech FM-310e microhardness tester was used to measure microhardness of the machined surface and subsurface of components with a 25 gf testing load. The hardness of each specimen was determined by taking the average of four measurements. Measurements were repeated three times to minimize any measurement error made by users.

3. Results and discussion

3.1. Machining performance results

3.1.1. Cutting temperature

Fig. 3 shows the recorded maximum cutting temperature variation as a function of cutting speeds under dry and cryogenic cooling conditions during machining of the Ni-rich NiTiHf alloy. It should be noted that it was not possible to make reliable measurements with the thermal camera under flood cooling conditions. Based on the results, it is evident that the contribution of cryogenic machining for reducing the cutting temperature is remarkable. Whereas the recorded maximum temperature was 262 °C in cryogenic machining, it was approximately 924 °C in dry machining at the lowest cutting speed.

Increasing cutting speed leads to increased cutting temperature in

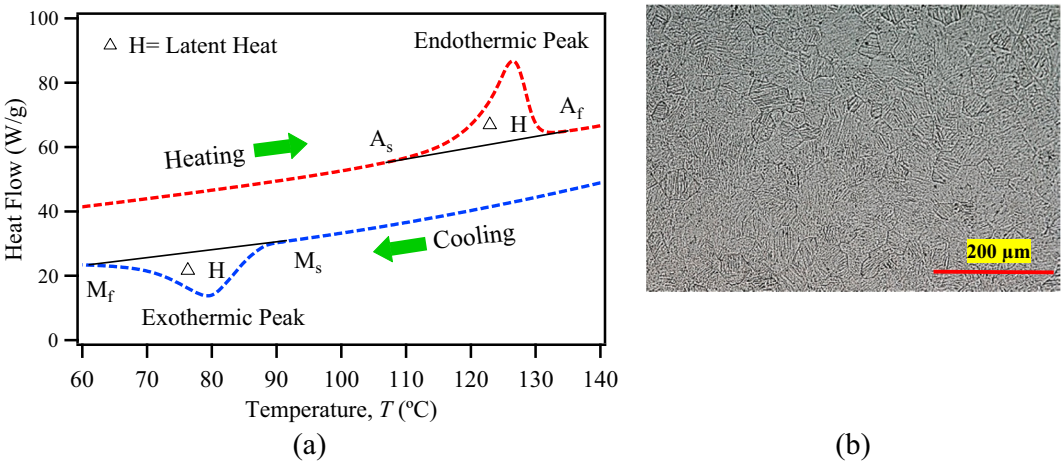

Fig. 1. (a) DSC results and (b) Optical microscopy images of the microstructure of the as-received NiTiHf alloy.

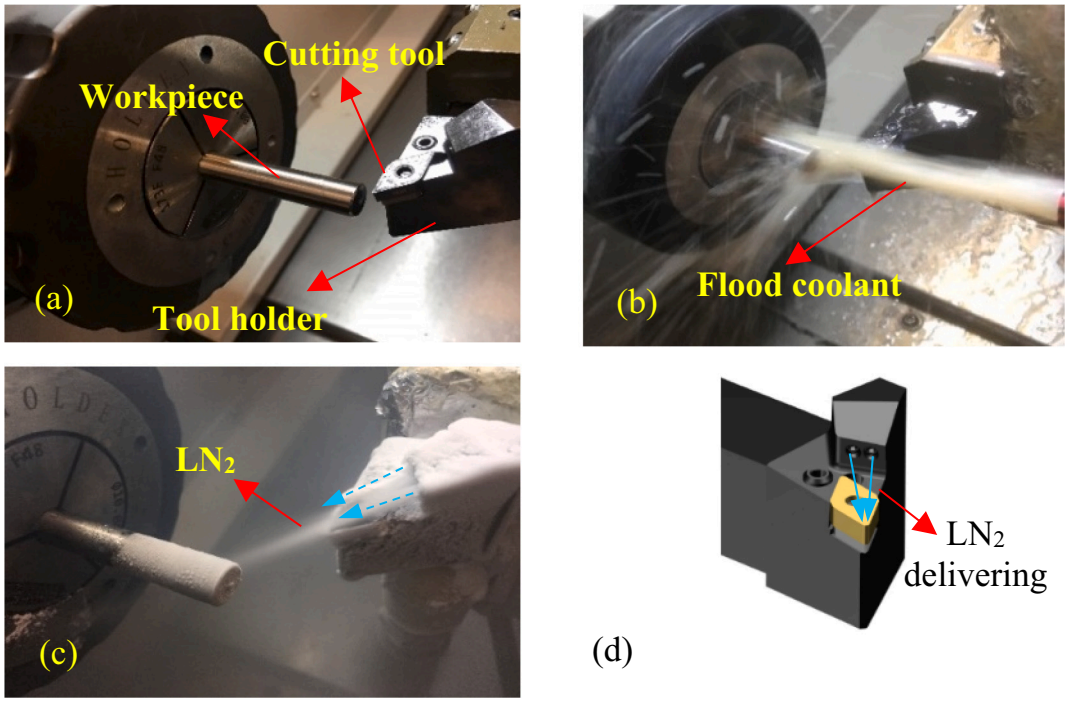

Fig. 2. (a) Dry cutting, (b) Flood cooling, (c) cryogenic machining, (d) delivering LN2 through PDJNL 2525M 11HP tool holder.

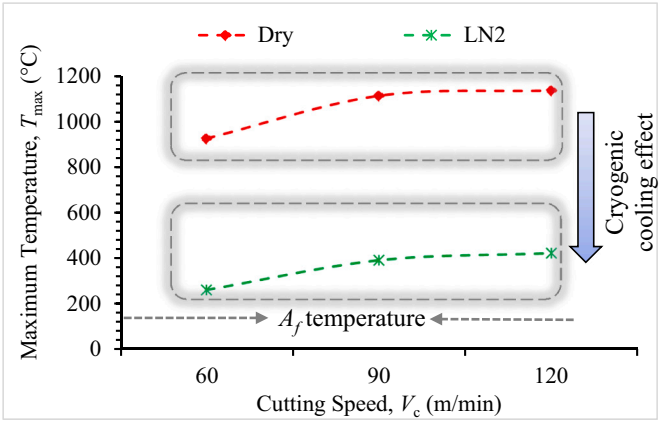

Fig. 3. Maximum temperature values occur at different cutting speeds and different cutting conditions.

both machining conditions. While the recorded temperature was approximately 1135 °C in dry cutting, it was 423 °C in cryogenic machining; this is 63% less than dry cutting at the highest cutting speed.

One of the issues in the machining process of advanced engineering materials is the extremely high temperature during the chip formation process, which occurs mainly because of the low thermal conductivity of these materials. Compared with other engineering materials, SMAs have very low thermal conductivity (8.6 W/m °C) [24] that results in increased temperature in the machining process, as shown in Fig. 3. Besides this aspect, phase transformation may also take place during the cutting process because of variation of the temperature. This also triggers the temperature in the cutting zone. This high cutting temperature is attributed to severe tool wear within a short time; this will be discussed in the following section.

Whereas high cutting temperature leads to the occurrence of some well-acknowledged issues in the machining process, additional issues with regard to the shape memory properties of SMAs should be examined, as phase transformation and shape memory properties are sensitive to the variation of temperature. DSC analysis presented in the method section confirms that phase transformation temperature (under stress-free conditions) of this NiTiHf alloy is 130 °C, but that temperature is not the only criterion determining the phase transformation of this alloy. A thermoelastic martensitic transformation is a mechanical process as well as a thermal transformation process [25]. Because of this combination, specific thermodynamic conditions have been established to express the effect of stress and temperature as external driving forces on the transformation by using the well-known Clausius-Clapeyron equation [25]:

$$\frac{d\sigma}{dT} = -\frac{\rho \Delta S}{\varepsilon_t} = -\frac{\rho \Delta H}{T_0 \varepsilon_t} \quad (1)$$

where ρ is the density of the transformation body, ΔS is the entropy change associated with the transformation, ε_t is the linear strain of the transformation in the direction of the uniaxial stress and T_0 is the equilibrium temperature. Considering this relation, it is obvious that an increase in transformation temperature occurs under stress [25] during the cutting process. Whereas austenite finish temperature was 130 °C, the recorded temperature at 60 m/min speed under cryogenic cooling was 262 °C, hence a difference of 132 °C.

3.1.2. Tool wear

Flank wear images and corresponding quantitative values are shown in Fig. 4 at various cutting conditions. Results indicate that tool wear increases with increase in cutting speed under all conditions. In addition, the amount of increasing wear with increasing cutting speed seemed to be affected significantly by the type of cooling strategy. The highest flank wear of 281 μm occurred when cutting at the lowest cutting speed of 60 m/min under dry conditions. Cryogenic cooling resulted in 86 μm flank wear, which is approximately 69% lower as compared with dry cutting.

Tool life becomes very short at a higher cutting speed (120 m/min), as tool wear reaches 689 μm under dry conditions. Flood cooling substantially helps to reduce flank wear at high speed. Cryogenic cooling at the highest cutting speed of 120 m/min significantly reduced flank wear, resulting in 53% less wear than under the dry cutting condition.

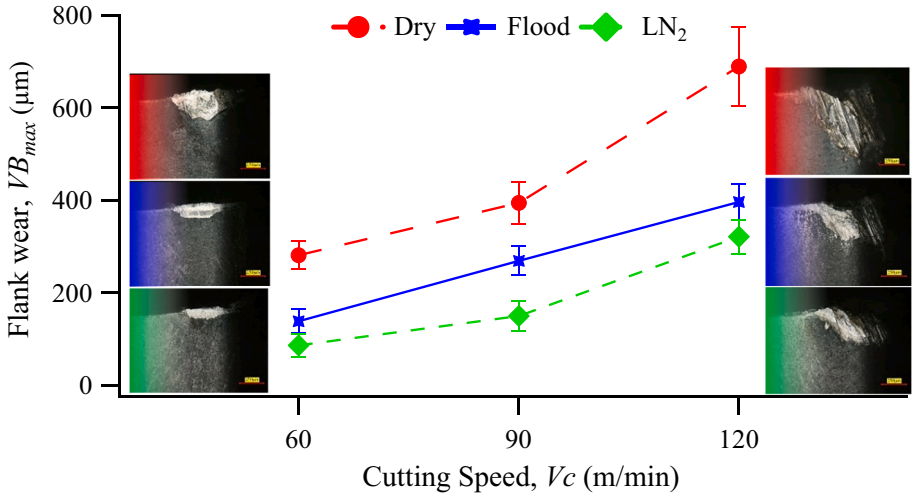

Fig. 4. Flank wear values on the cutting tool at different cutting speeds and cutting conditions.

Overall, these results provide strong evidence that Ni-rich NiTiHf is an extremely difficult-to-machine material, even under flood and cryogenic cooling conditions, when flank wear response as a function of cutting speed is taken into account.

Many parameters can affect tool wear, including the hardness of the insert and the workpiece material, the machining parameters and the working temperature of the cutting tool. Commonly observed tool wear mechanisms operating on cemented carbide tools when machining high-temperature alloys are diffusion [26–28], adhesion [27,29] and abrasion [27]. The dominant mechanism observed on the worn tools used in this study was abrasive wear, as shown in Fig. 5(a). Parallel grooves are strong evidence of abrasive wear. It is thought that mechanical abrasive wear on the cutting tool was due to the microscopic hard abrasives within the material, such as HfO_2 oxides [30] (the white dots in Fig. 4 (b)). The HfO_2 particles in the workpiece are presented in Fig. 5 in the extrusion direction. HfO_2 particles are circular, and the maximum size was measured as 3 µm.

Machining under dry conditions at the highest cutting speed of 120 m/min resulted in the highest flank wear, 689 µm, with high volumetric loss as compared with other cooling conditions. At this condition, the cutting temperature exceeded 1100 °C, reaching the softening temperature of the carbide tool [31] and thus deteriorating its geometry, as

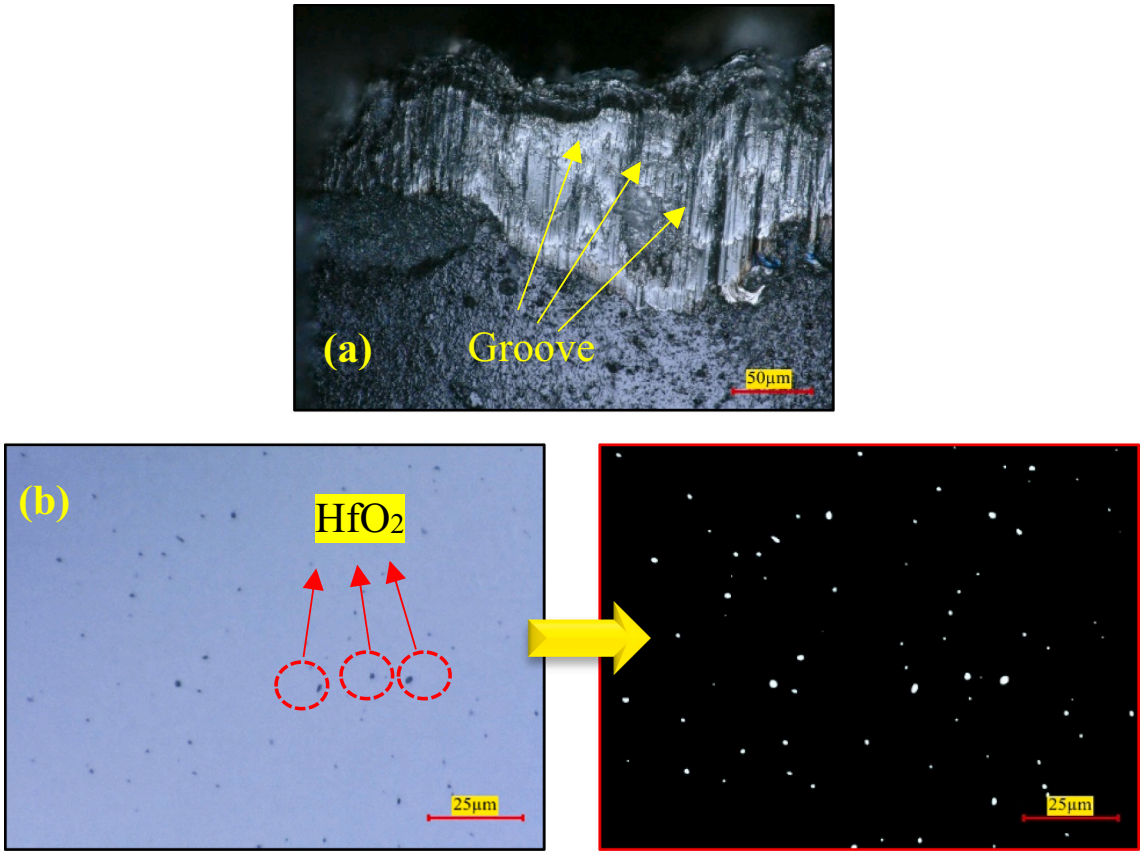

Fig. 5. (a) Worn surface of cutting tool, (b) HfO_2 particles in the material.

shown in Fig. 4. This volumetric loss is much lower under other cutting conditions. This situation can be attributed to the effect of high temperature on the hardness of the cutting tool, both the carbide substrate and the coatings, as shown in Fig. 6. It was clearly shown that the hardness of the TiAlN coating drops almost linearly with an increase in temperature, whereas a sudden decrease in hardness of the carbide substrate occurs after 600 °C. As for the cryogenic cutting conditions, the generated cutting temperature was below 600 °C, as shown in Fig. 3, thus the cutting tools experienced less volumetric loss and lower geometry deterioration.

When the ISO3684:1994 standard for tool life criteria is considered (300 μm at finish machining), the cutting tools have reached their tool life at cutting speeds of 90 m/min and above under dry cutting conditions. At the highest cutting speed of 120 m/min, the cooling condition that prolonged the cutting time of the tool below the tool life criterion was cryogenic cooling. This finding suggests that liquid nitrogen can suppress the cutting temperature below 600 °C, thus maintaining tool hardness and eventually improving cutting tool performance during machining.

Nose wear is also observed during machining of high-temperature shape memory alloy NiTiHf. An increase in flank and nose wear tends to disrupt the quality of the treated surface, creating a rougher surface. In addition, nose wear directly affects radial force [15]. The progression of cutting-tool nose wear at various cutting conditions shows a linear trend, as presented graphically in Fig. 7. The effect of cutting speed and cooling conditions on wear is obvious. At the lowest cutting speed of 60 m/min, the highest amount of nose wear (85 μm) was recorded under dry cutting conditions. At other cooling conditions, the average nose wear was approximately 23% lower. At highest cutting speed of 120 m/min, the differences in the amount of nose wear under various cooling conditions were obvious. The maximum nose wear of 547 μm was recorded at a cutting speed of 120 m/min under dry conditions. Under flood conditions, the recorded nose wear of the cutting tool was 420 μm, approximately 23% less than under dry cutting conditions. The least amount of nose wear, 328 μm, was obtained under cryogenic cooling conditions, which is approximately 40% lower than the amount of nose wear formed under dry cutting conditions.

It was observed that volume loss and disruption in the cutting tool geometry occur at the highest cutting speed of 120 m/min. To further examine the volumetric loss of the cutting edge, the cutting tools were scanned in three dimensions and profile sections were taken using a digital optical microscope. The profile lines of the cutting tools were graphically created and are presented in Fig. 7. The outer black line represents the original profile of the fresh cutting tool. The volumetric loss occurring in the cutting tools under different cooling conditions is seen in the images. This result also shows that the largest volumetric loss takes place with dry machining.

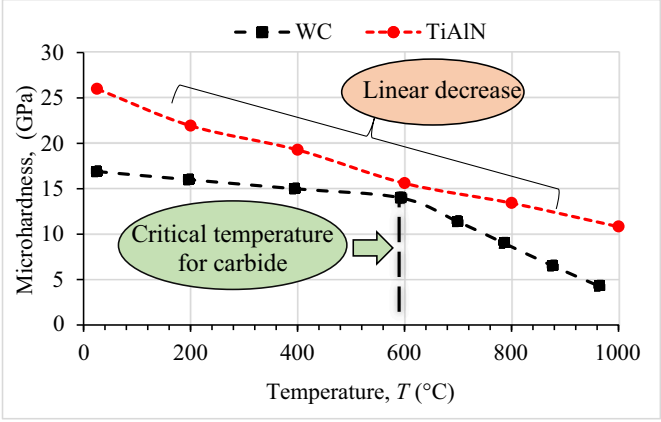

Fig. 6. Hardness change of carbide tool and TiAlN coating at different temperatures [31].

3.1.3. Cutting forces

The main cutting force (F_c) acting on the cutting tool during the turning operation of high-temperature SMA NiTiHf is shown in Fig. 8. Results showed that cutting speed and cooling conditions significantly affect the cutting force. Under all conditions investigated, the cutting force shows an increasing trend with an increase in cutting speed. This phenomenon occurred due to the increase in stress of the work material with increase in cutting speed, thus accelerating the wear rate of the cutting edge of the tool. During the cutting test at the lowest cutting speed (60 m/min), the highest cutting force was observed to occur under dry cutting conditions.

The recorded tool life was also low at this condition as a result of the high cutting temperature generated during dry cutting, and the cutting force increased accordingly. Under flood coolant, a 29% reduction in cutting force over the dry cutting condition was recorded. Meanwhile, 48% lower force was recorded for the cryogenic cooling condition than for the dry cutting condition.

For comparison and further explanation, the results of the main cutting force (F_c) at 60 m/min for both dry cutting and cryogenic cooling conditions are shown in Fig. 8. Results clearly show that cutting force continuously increases with the increment of cutting time. At the beginning of the machining test, the cutting force was found to be lower for dry machining as compared with cryogenic machining. However, after 4 s, the cutting force for dry cutting starts to increase gradually, whereas cryogenic cooling remains constant until the end of the test. The significant variation in cutting force between the dry and cryogenic machining comes from the progression of tool wear.

Experimental results also showed that at cutting speed above 60 m/min, the highest cutting force occurred under dry cutting conditions. It was observed that the influence of tool wear on cutting force is more dominant as compared with cutting speed. Under flood conditions, approximately 5% lower cutting force was recorded than for the dry cutting condition. Under cryogenic cooling, 11% lower cutting force was recorded as compared with dry cutting.

3.2. Surface integrity measures

3.2.1. Surface quality

Surface quality is an essential feature required in the aviation and aerospace industries. After the machining tests, the surface roughness of each specimen was measured. Results are presented in Fig. 9. At a cutting speed of 60 m/min, the highest roughness value of 0.67 μm was recorded when machining under dry conditions. In comparison, roughness values under flood and LN_2-assisted cooling conditions were 38% and 20% lower, respectively. At the highest cutting speed of 120 m/min, the highest surface roughness value of 5.6 μm was recorded under dry cutting conditions. This high surface roughness was due to the effect of the high amount of wear on the cutting edge of the tool when machining under dry conditions. Flank and nose wear of cutting tools measured after dry machining was quite high as compared with wear under cryogenic and flood cooling. High volume loss also disrupts the cutting tool geometry. A deep groove on the nose region of the cutting tool was observed at a cutting speed of 120 m/min. The high surface roughness and poor surface topography result from the extreme and rapid wear, and hence geometrical disruption, of the cutting tool in dry machining. At the same cutting speed, the roughness value under flood conditions was 1.6 μm, 71% lower than the value recorded under dry cutting conditions. The lowest surface roughness value of 1.3 μm was obtained under cryogenic conditions; this is approximately 77% lower than the value recorded under dry cutting conditions.

Fig. 9 also shows the calculated arithmetical surface roughness, derived using the following empirical formula [32]:

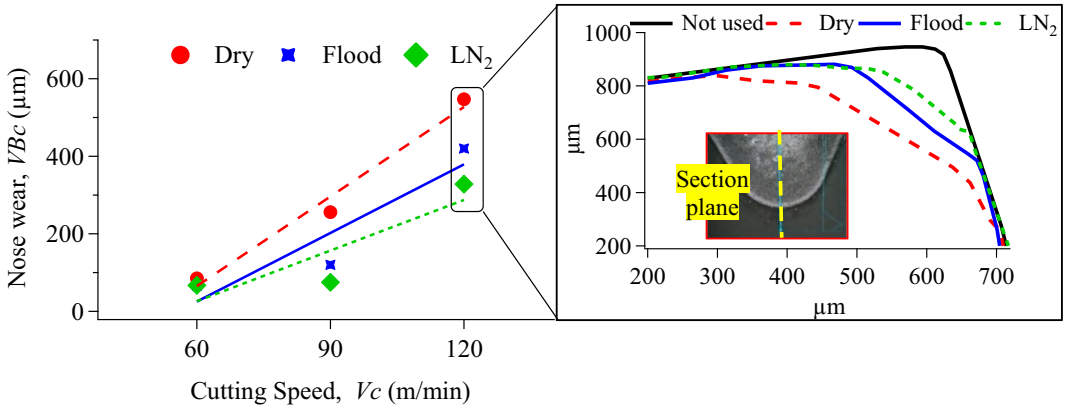

Fig. 7. Nose wear values at different cutting speeds and different cooling conditions. Profile lines of the tool at 120 m/min cutting speed.

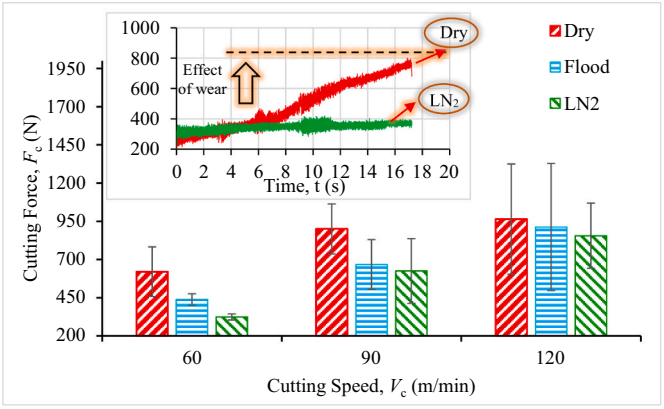

Fig. 8. Variation of cutting force as a function of cutting speed under different cooling conditions.

$$R_a = \frac{0.0321 x f^2}{r_c} \quad (2)$$

where f represents feed rate and r_c represents nose radius of the cutting tool. Experimental data shows that increased cutting speed results in increased surface roughness. The calculated surface roughness value for these cutting parameters and the cutting tool was approximately 0.39 µm.

3.2.2. Microhardness

SMAs are sensitive to changes of temperature and stress. Their shape memory response is also stress and temperature dependent. Because the surface and subsurface of machined components are subjected to stress and temperature during the chip formation process, the machining process has a high potential to influence the surface characteristics of such alloys. One of the common ways to determine the influences of the chip formation process on the surface aspects is to examine the microhardness of the surface and subsurface of the machined specimen to determine the depth of the machining-induced layer. Measured microhardness on the surface and subsurface of specimens machined under dry, flood and cryogenic machining is presented in Fig. 10. The average hardness of the as-received specimen was approximately 395 ± 5 HV. Fig. 10 shows that the machining process under dry, flood, and cryogenic cooling conditions results in increased hardness on the surface and subsurface. Machining alters the depth 100 µm below the surface of the specimen. The machining process generates high strain and temperature [33], thus the machined surface is subjected to large strains, high strain rates and high temperatures. Once liquid nitrogen is delivered to the cutting region during the chip formation process, the surface becomes very cold. This cold deformation results in large residual stress, and the surface retains strain due to the increased dislocation density [34].

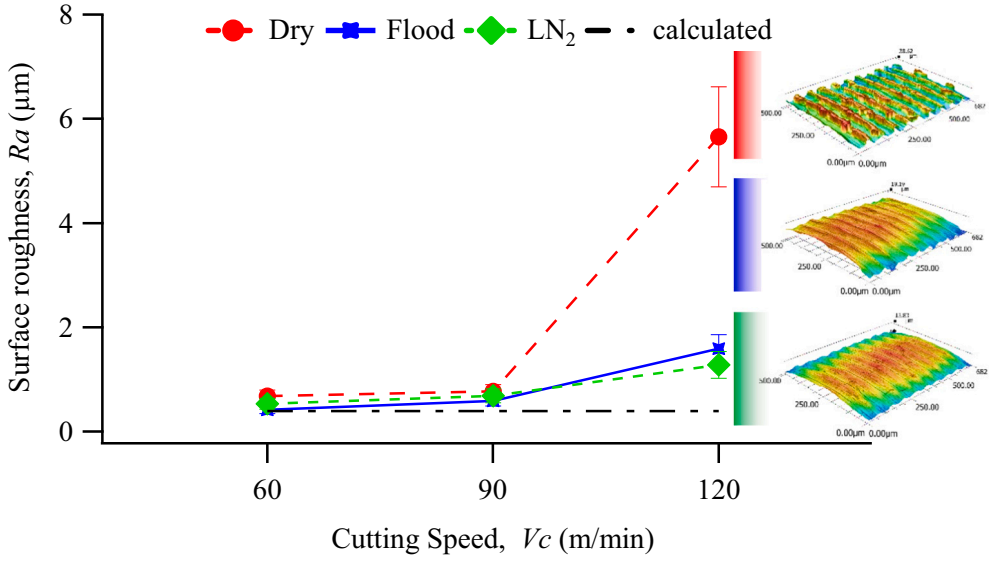

Fig. 9. Measured and calculated average surface roughness of the machined surface of the NiTiHf alloy.

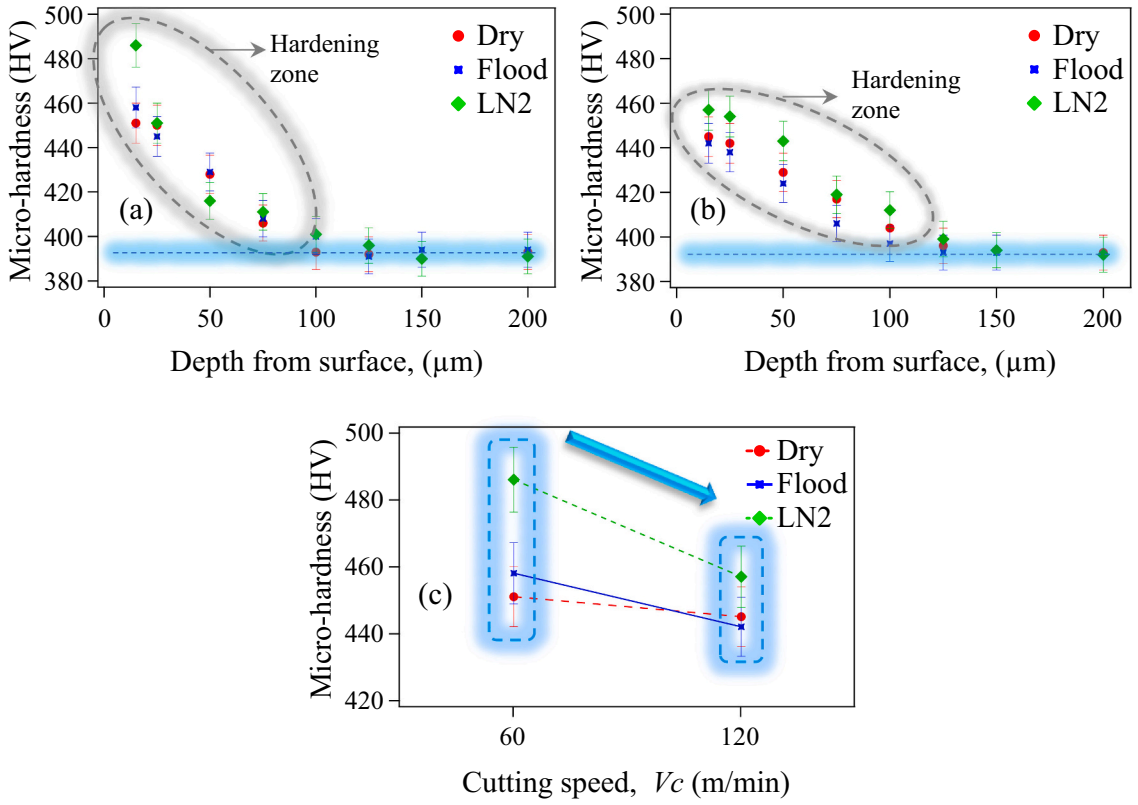

Fig. 10. Subsurface microhardness of dry, flood and cryogenically machined NiTiHf alloy at (a) 60 m/min and (b) 120 m/min, (c) microhardness at 15 μm depth from the surface of the machined parts.

Consequently, measured hardness under cryogenic cooling is much larger than under dry and flood cooling. During dry and flood cooling, due to the temperature, partial annihilation in the microstructure is expected, and this phenomenon will eventually reduce the density of dislocation resulting from the machining process. The lower the machining temperature, the higher the hardness. This statement is also supported by the effect of cutting speed on microhardness. The highest hardness in all conditions was measured from the specimen machined at the lowest cutting speed (60 m/min), as seen in Fig. 10(c). Deformation temperature clearly plays a dominant role in determining the percentage

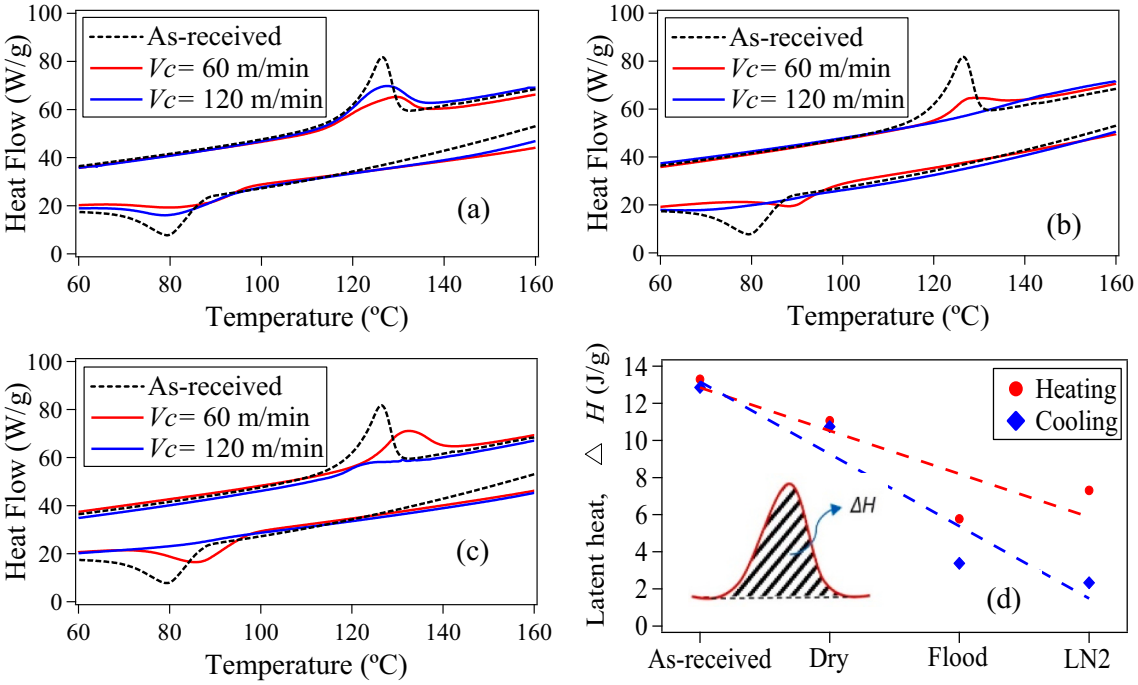

Fig. 11. DSC responses of (a) dry, (b) flood cooling, (c) cryogenically machined parts, (d) Latent heat (ΔH) of samples (Vc = 120 m/min).

of retained energy on the surface and subsurface of machined specimens. This relationship is also validated by the DSC analysis results presented in Fig. 11.

3.2.3. Phase transformation response and latent heat for transformation

Phase transformation response is the main functional performance parameter of SMAs. Thus, it is necessary to examine the phase transformation response of the cutting-induced layer to determine the effects of the machining process on the functional performance of NiTiHf SMAs. Fig. 11 shows the DSC response of specimens machined under various conditions and two cutting speeds in comparison with the as-received specimen. Fig. 11(d) depicts latent heat for transformation (ΔH) of these specimens. According to the DSC analysis, the transformation peaks of machined specimens show profound broadening as compared with the peaks of as-received specimens at both cutting speeds. Peak broadening is much larger at high speed (120 m/min) for all cutting conditions. Transformation temperature at 60 m/min cutting speed can be easily measured from the DSC graph. Whereas A_f temperature for the as-received specimen is 130 °C, it is 137 °C for the dry-machined specimen, 141 °C for the cryogenically machined specimen and 143 °C for the specimen machined with flood cooling. The increase in transformation temperature with the machining process varies from 5 to 10% depending on cutting condition. Shifts can also be observed when A_s, M_s and M_f temperatures of machined specimens are measured. To the authors' best knowledge, this current work is the first study illustrating machining-induced altered transformation temperature of NiTiHf high-temperature SMAs. The surface and subsurface of the specimens are subjected to stress, leaving residual stress on these regions. This stress affects both the microhardness results, as presented in Fig. 10, and the transformation temperature of the material. As DSC analysis of the machined specimens showed, the energy required for transformation is therefore decreased. As the area of peak represents the latent heat for the transformation (ΔH), the large difference between as-received specimens and specimens machined at 120 m/min cutting speed can be seen in Fig. 11(d). The as-received material is approximately 13.29 J/g (endothermic) and 12.85 J/g (exothermic) during heating and cooling, respectively. But these values were found as 11.06 J/g (endothermic) and 10.74 J/g (exothermic) for the dry-machined specimen, 5.77 J/g (endothermic) and 3.38 J/g (exothermic) for the specimen machined under flood cooling and 7.31 J/g (endothermic) and 2.33 J/g (exothermic) for the cryogenically machined specimen. Whereas the latent heat for transformation during heating varies from approximately 16 to 56%, the latent heat for transformation during cooling varies from approximately 16 to 81%. It is seen that flood and cryogenic cooling have a much deeper influence on latent heat for transformation. During the cutting process, deforming the surface of the NiTiHf alloy at a relatively low temperature suppresses the annihilation effect on the surface and subsurface, altering transformation temperature and latent heat for transformation as compared with the as-received specimens. In contrast, under dry machining conditions, elevated temperatures trigger the annihilation mechanism and eventually relatively reduce the effect of surface deformation on transformation temperature and latent heat for transformation.

Because the machining process, particularly flood and cryogenic cooling, alters the latent heat response of the surface and subsurface as well as the transformation temperature of the specimens, it also alters the overall transformation response of the specimens. The following equation indicates the parameters for the transformation [35]:

$$f_t(\nu_M, \Sigma, T) = \Sigma - \frac{\lambda_T}{T_0}(T - T_0) - h\nu_M \tag{3}$$

where Σ is the effective stress at the Gauss point. The equilibrium transformation temperature $T_0 = M_s + A_f/2$ indicates volume fraction for the transformation, h indicates transformation hardening value and λ_T is the latent heat per unit reference volume. Based on this relation and the results presented in Fig. 11, it is possible to conclude that specimens machined using flood and cryogenic cooling will rarely have the same transformation response. As previously noted, the machining process also altered transformation temperatures, including M_s and A_f. Therefore, the equilibrium temperature of machined specimens, particularly flood and cryogenically machined specimens, will be different from as-received specimens.

4. Conclusions

This work shows the effect of cooling, specifically cryogenic and flood cooling, on machining performance and shape memory properties of Ni-rich NiTiHf alloys. Results were compared with those obtained from dry machining. The critical findings can be summarized as follows:

- The results presented in this paper demonstrate the effectiveness of cryogenic cooling in improving the machinability of Ni-rich NiTiHf by reducing cutting temperature, tool wear, force components and surface roughness.
- Although flood cooling offers advantages over dry cutting in terms of machinability of Ni-rich NiTiHf, its contribution is not as significant as that of cryogenic cooling.
- Strain hardening on the surface and subsurface of the NiTiHf alloy occurs as a result of the machining process and results in increased surface hardness of machined parts.
- This present work demonstrates that the machining process alters shape memory properties of Ni-rich NiTiHf high-temperature shape memory alloys. Depending on the cutting condition, the transformation temperature of machined specimens increases between 5 and 10% as a result of the machining process.
- Latent heat for transformation of machined specimens is also altered, from 16 to 56% during heating and from 16 to 81% during cooling. This variation creates inhomogeneous shape memory properties throughout the cross section of machined specimens.
- Considering the effect of machining under dry and cooling conditions, machined Ni-rich NiTiHf parts must be heat treated to homogenize the microstructure.

Declaration of competing interest

The authors declare that they have no known competing financial interests or personal relationships that could have appeared to influence the work reported in this paper.

Acknowledgments

The authors sincerely acknowledge the financial support from TUBITAK (The Scientific and Technological Research Council of Turkey) under project number 116M346. O.B. acknowledges support from the NASA Aeronautics Research Mission Directorate (ARMD) Transformational Tools & Technologies (TTT) project. The authors also thank Marmara University and Universiti Teknologi Malaysia for the collaboration and assistance in conducting this research through the research university grants 00P23 and 08G37.

References

[1] Hayrettin C, Karakoc O, Karaman I, Mabe J, Santamarta R, Pons J. Two way shape memory effect in NiTiHf high temperature shape memory alloy tubes. Acta Mater 2019;163:1–13.
[2] Evirgen A, Karaman I, Santamarta R, Pons J, Noebe R. Microstructural characterization and superelastic response of a Ni50. 3Ti29. 7Zr20 high-temperature shape memory alloy. Scr Mater 2014;81:12–5.
[3] Benafan O, Garg A, Noebe R, Bigelow G, Padula II S, Gaydosh D, Schell N, Mabe J, Vaidyanathan R. Mechanical and functional behavior of a ni-rich ni 50.3 Ti29.7 Hf20 high temperature shape memory alloy. Intermetallics 2014;50:94–107.

[4] Benafan OB, Calkins J, Kumar FT, Stebner P, Turner A, Vaidyanathan T, Webster R, Young J, ML. Shape memory alloy actuator design: Casmart collaborative best practices. In: ASME 2011 Conference on Smart Materials; 2011. p. 18–21.
[5] Weinert K, Petzoldt V. Machining of NiTi based shape memory alloys. Mater Sci Eng A 2004;378:180–4.
[6] Weinert K, Petzoldt V, Kötter D. Turning and drilling of NiTi shape memory alloys. CIRP Annals-Manufacturing Technology 2004;53:65–8.
[7] Velmurugan C, Senthilkumar V, Dinesh S, Arulkirubakaran D. Machining of NiTi-shape memory alloys-a review. Mach Sci Technol 2018;22:355–401.
[8] Hassan M, Mehrpouya M, Dawood S. Review of the machining difficulties of nickel-titanium based shape memory alloys. Appl Mech Mater 2014;564:533.
[9] Weinert K, Petzoldt V, Kötter D. Turning and drilling of NiTi shape memory alloys. CIRP Ann Manuf Technol 2004;53:65–8.
[10] Benafan O. Deformation and phase transformation processes in polycrystalline NiTi and NiTiHf high temperature shape memory alloys. 2012.
[11] Kirmacioglu KE, Kaynak Y, Benafan O. Machinability of ni-rich NiTiHf high temperature shape memory alloy. Smart Mater Struct 2019;28:055008.
[12] Kabil A, Kaynak Y, Saruhan H, Benafan O. Multi-objective optimization of cutting parameters for machining process of Ni-rich NiTiHf high-temperature shape memory alloy using genetic algorithm. Shape Memory Superelasticity 2021:1–10.
[13] Zhao Y, Li J, Guo K, Sivalingam V, Sun J. Study on chip formation characteristics in turning NiTi shape memory alloys. J Manuf Process 2020;58:787–95.
[14] Kaynak Y, Karaca H, Jawahir I. Cutting speed dependent microstructure and transformation behavior of NiTi alloy in dry and cryogenic machining. J Mater Eng Perform 2015;24:452–60.
[15] Kaynak Y, Karaca HE, Noebe RD, Jawahir IS. Tool-wear analysis in cryogenic machining of NiTi shape memory alloys: a comparison of tool-wear performance with dry and MQL machining. Wear 2013;306:51–63.
[16] Zhao Y, Guo K, Li J, Sun J. Investigation on machinability of NiTi shape memory alloys under different cooling conditions. Int J Adv Manuf Technol 2021;116:1913–23.
[17] Miller T, Gupta K, Laubscher R. An experimental study on MQL assisted high speed machining of NiTi shape memory alloy. In: Proceedings of 16th international conference on manufacturing research; 2018. p. 80–5.
[18] Khalil ANM, Azmi AI, Murad MN, Ali MAM. The effect of cutting parameters on cutting force and tool wear in machining nickel titanium shape memory alloy ASTM F2063 under minimum quantity nanolubricant. Procedia CIRP 2018;77:227–30.
[19] Mehta K, Gupta K. Machining of shape memory alloys. In: Fabrication and processing of shape memory alloys. Springer; 2019. p. 9–37.
[20] Abidin ZZ, Mativenga PT, Harrison G. Chilled air system and size effect in micro-milling of nickel– titanium shape memory alloys. Int J Precis Eng ManufGreen Technol 2020;7:283–97.
[21] Shah P, Bhat P, Khanna N. Life cycle assessment of drilling inconel 718 using cryogenic cutting fluids while considering sustainability parameters. Sustain Energy Technol Assess 2021;43:100950.
[22] Agrawal C, Khanna N, Pruncu CI, Singla AK, Gupta MK. Tool wear progression and its effects on energy consumption and surface roughness in cryogenic assisted turning of ti-6Al-4V. Int J Adv Manuf Technol 2020;111:1319–31.
[23] A. F2004-05(2010). Standard Test Method for Transformation Temperature of Nickel-Titanium Alloys by Thermal Analysis. ASTM International; 2010.
[24] Shaw JA. Simulations of localized thermo-mechanical behavior in a NiTi shape memory alloy. Int J Plasticity 2000;16:541–62.
[25] Liu Y, Mahmud A, Kursawe F, Nam T-H. Effect of pseudoelastic cycling on the clausius-clapeyron relation for stress-induced martensitic transformation in NiTi. J Alloys Compd 2008;449:82–7.
[26] Zhang S, Li JF, Deng J, Li Y. Investigation on diffusion wear during high-speed machining ti-6Al-4V alloy with straight tungsten carbide tools. Int J Adv Manuf Technol 2009;44:17.
[27] Venugopal K, Paul S, Chattopadhyay A. Growth of tool wear in turning of ti-6Al-4V alloy under cryogenic cooling. Wear 2007;262:1071–8.
[28] Jawaid A, Sharif S, Koksal S. Evaluation of wear mechanisms of coated carbide tools when face milling titanium alloy. J Mater Process Technol 2000;99:266–74.
[29] Hao Z, Gao D, Fan Y, Han R. New observations on tool wear mechanism in dry machining Inconel 718. Int J Mach Tool Manuf 2011;51:973–9.
[30] Arsecularatne J, Zhang L, Montross C. Wear and tool life of tungsten carbide, PCBN and PCD cutting tools. Int J Mach Tool Manuf 2006;46:482–91.
[31] Ezugwu E. High speed machining of aero-engine alloys. J Braz Soc Mech Sci Eng 2004;26:1–11.
[32] Hagiwara M, Chen S, Jawahir I. Contour finish turning operations with coated grooved tools: optimization of machining performance. J Mater Process Technol 2009;209:332–42.
[33] Oxley P. Mechanics of machining. Chichester: Ellis Horwood; 1989.
[34] De la Flor S, Urbina C, Ferrando F. Effect of mechanical cycling on stabilizing the transformation behaviour of NiTi shape memory alloys. J Alloys Compd 2009;469:343–9.
[35] Kaynak Y, Manchiraju S, Jawahir I. Modeling and simulation of machining-induced surface integrity characteristicsof NiTi alloy. Procedia CIRP 2015;31:557–62.